

Polarization Lidar For Shallow Water Depth Measurement

Steven Mitchell,^{1,*} Jeffrey Thayer,¹ and Matthew Hayman²

¹*University of Colorado, Department of Aerospace Engineering Sciences, Boulder, Colorado,
80309, USA*

²*University of Colorado, Department of Electrical, Computer and Energy Engineering, Boulder,
Colorado, 80309, USA*

**Corresponding author: Steven.Mitchell@colorado.edu*

A bathymetric, polarization lidar system transmitting at 532 nanometers and using a single photomultiplier tube is employed for applications of shallow water depth measurement. The technique exploits polarization attributes of the probed water body to isolate surface and floor returns, enabling constant fraction detection schemes to determine depth. The minimum resolvable water depth is no longer dictated by the system's laser or detector pulse width and can achieve better than an order of magnitude improvement over current water depth determination techniques. In laboratory tests, a Nd:YAG microchip laser coupled with polarization optics, a photomultiplier tube, a constant fraction discriminator and a time to digital converter are used to target various water depths. Measurement of 1 centimeter water depths with an uncertainty of ± 3 millimeters are demonstrated using the technique. This novel approach enables new approaches to designing laser bathymetry systems for shallow depth determination while not compromising deep water depth determination.

OCIS codes: 010.3640, 120.0280, 240.5445, 280.1355, 280.3640.

Introduction

Advancements in light detection and ranging (lidar) have enabled measurement of increasingly shallow water depths (< 2 meters) for collection of bathymetric data [1,2]. Present day bathymetry lidar systems are capable of depth measurements down to tens of centimeters [3,4,5]. The limit to achieving shallower depth measurements is related to the applied technique and the imposed demands for short laser pulse widths and rapid detector response times. Additional limits are imposed in the instance of requisite signal analysis of analog-to-digital converted waveforms. A demonstration of such waveform analysis under shallow water conditions using signal returns generated by Raman scattering in the water column has been presented [6]. The signal return waveform is the convolution of backscattered nanosecond laser pulses from the water with detector response times that, together, constitute the instrument bandwidth. Invariably, current techniques for determining shallow water depth are inhibited by the overall instrument bandwidth. For shallow waters such as those often found along the shoreline of glacial meltponds, limited instrument bandwidth results in ambiguities between surface reflections, volume backscatter, and floor returns making water depth indeterminable. Future developments of picosecond pulse width lasers and fast detectors can further improve shallow water measurement capabilities, but at greater cost and complexity. Ultimately these techniques will be limited due to physical dispersion of the water.

This paper introduces a new approach to shallow water depth determination by exploiting the differing polarization attributes of scattered signals from the water surface, volume and floor. The polarization preserving nature of backscattered laser light from the water surface and volume, as well as the depolarizing nature of backscattered laser light from rough floor topographies has been demonstrated [7]. Thus signal returns from the floor can be isolated from

surface and volume returns through polarization discrimination at sub-pulse width resolution. This approach effectively shifts the dependency away from instrument bandwidth and places the demand on the timing electronics, where constant fraction detection of separated surface and floor signals can produce accurate timing resolution. This approach enables accurate determination of time of flight differences between polarized and depolarized returns to produce better than an order of magnitude improvement in shallow water depth measurement. The approach of discriminating polarized lidar return signals within the pulse width provides a single wavelength solution to shallow water bathymetric ambiguities that is no longer limited by laser and/or detector pulse widths. As will be demonstrated in subsequent sections of this paper, these attributes facilitate measurement of water depth to single centimeters and less.

Technique

The fundamental instrument setup for the technique described here is illustrated in Figure 1. The transmitter consists of a 532 nanometer linearly polarized laser. A half-wave plate is used to rotate the linearly polarized light exiting the laser head into alignment with the vertical transmission axis of a 532 nanometer polarizing beam splitter (PBS) cube. The vertically co-polarized laser light exiting the PBS passes through a quarter-wave plate which is free to rotate about the optical axis. When the fast axis of the quarter-wave plate is oriented 45 degrees to the linear polarization output of the cube, the quarter-wave plate retards the linear slow polarization component relative to the fast polarization component by 90 degrees, emitting left-hand circularly polarized light towards the target water body.

When incident upon the water surface and column, the transmitted circularly polarized light reflects back to the receiver in a nearly preserving, but opposite, circular polarization state. This polarization, 180 degrees out of phase from the transmitted state, is retarded again by the

45-degree oriented quarter-wave plate. The result is linearly polarized light incident upon the PBS, rotated about the optical axis by 90 degrees (horizontal) into the reflection axis of the PBS to a photomultiplier tube (PMT) for detection.

Rotating the quarter-wave plate to align the fast and slow axes to the PBS transmission plane, no relative phase shift is imposed by the quarter-wave plate. As a result, vertically polarized laser light is transmitted to the water. The surface and column are polarization preserving, reflecting light that is primarily in the vertical plane. This linearly polarized light passes through the quarter-wave plate unmodified so that the PBS does not reflect the light into the receiving channel. However, when incident upon the floor, the transmitted linearly polarized light depolarizes upon reflection due to the rough topography. The quarter-wave plate has no impact on the backscattered unpolarized light, of which half is reflected by the PBS to the detector in the receiver.

Through discrimination of the reflected signal polarization state between laser firings, the lidar transition between reception of water and floor backscatter is dictated by the orientation of the quarter-wave plate. Rotation of the quarter-wave plate permits the receiver to transition between detection of either state, even when surface and floor returns are contained within each return pulse. As such, the body of water can be effectively removed from the return signal, enabling the depolarized floor signals to be isolated for analysis. This can either be performed on a predetermined pulse to pulse basis as applicable to the presently described compact single telescope and detector system, or simultaneously by including a separate receiving telescope with two detectors. In an effort to generate the most compact, less complex, and inexpensive instrument design, the polarization discrimination between signals is performed in this paper on a pulse to pulse basis using a single telescope and detector.

Simulation

Shallow water bathymetry using the setup in Figure 1 is dictated by the quarter-wave plate orientation and subsequent modification of transmitted and received polarization states. An analytical description of the technique begins by defining the associated Stokes vector of the linearly polarized laser pulse, \vec{S}_{Tx} , oriented using a half-wave plate for maximum transmission through the polarizing beam splitter cube.

$$\vec{S}_{Tx} = \begin{bmatrix} 1 \\ -1 \\ 0 \\ 0 \end{bmatrix} \quad (1)$$

An arbitrary wave plate of phase shift γ and fast axis orientation θ is described using Mueller matrices as

$$VWP(\theta, \gamma) = \begin{bmatrix} 1 & 0 & 0 & 0 \\ 0 & \cos^2(2\theta) + \cos(\gamma)\sin^2(2\theta) & \cos(2\theta)\sin(2\theta) - \cos(2\theta)\sin(2\theta)\cos(\gamma) & -\sin(2\theta)\sin(\gamma) \\ 0 & \cos(2\theta)\sin(2\theta) - \cos(2\theta)\sin(2\theta)\cos(\gamma) & \cos(\gamma)\cos^2(2\theta) + \sin^2(2\theta) & \cos(2\theta)\sin(\gamma) \\ 0 & \sin(2\theta)\sin(\gamma) & -\cos(2\theta)\sin(\gamma) & \cos(\gamma) \end{bmatrix} \quad (2)$$

with a half-wave plate γ of π radians oriented to θ_H and quarter-wave plate γ of $\pi/2$ radians oriented to θ_Q .

The PBS is modeled as a polarizer oriented to θ_P of 0 degrees for transmission along the vertical axis in the instrument transmitter and oriented to $\theta_P + 90$ degrees for horizontal transmission in the receiver.

$$Pol(\theta) = \begin{bmatrix} 0.5 & 0.5 \cos(2\theta) & -0.5 \sin(2\theta) & 0 \\ 0.5 \cos(2\theta) & 0.5 \cos^2(2\theta) & -0.5(\cos(2\theta)\sin(2\theta)) & 0 \\ 0.5 \sin(2\theta) & 0.5(\cos(2\theta)\sin(2\theta)) & -0.5 \sin^2(2\theta) & 0 \\ 0 & 0 & 0 & 0 \end{bmatrix} \quad (3)$$

During acquisition of bathymetric measurements, the quarter-wave plate is initially oriented to θ_Q of 45 degrees for transmission of circularly polarized light towards the target. After an arbitrary number of laser firings in this orientation, the quarter-wave plate is rotated to θ_Q of 0 degrees for transmission of vertical linear polarization during a second set of laser firings. In both orientations the backscattered light propagates in the opposite direction from the transmit path, such that the quarter-wave plate is expressed with orientation of $-\theta_Q$ during signal reception.

Combining the transmitted Stokes vector in (1) with the appropriate Mueller matrices described in (2) and (3), as depicted by the system layout in Figure 1, produces the received Stokes vector

$$\vec{S}_{Rx} = \left[Pol(\theta_P + 90) \cdot VWP(-\theta_Q, \pi/2) \cdot M_{target} \cdot VWP(\theta_Q, \pi/2) \cdot Pol(\theta_P) \cdot VWP(\theta_H, \pi) \right] \vec{S}_{Tx} \quad (4)$$

with the intensity measured by the PMT defined as

$$I_{Rx} = [1 \ 0 \ 0 \ 0] \vec{S}_{Rx} \quad (5)$$

The Mueller matrix M_{target} represents the scattering phase function of the water target. In these simulations, and in the design of our measurements, the depolarizing components of the scattering matrix will be the main focus. This is attributed to the observation of strong depolarization caused by coastal shorelines [7] and our observations of strong depolarization by

ice. As such, the scattering matrix takes the form of a normalized depolarization matrix given by [8]

$$M_{target} = \begin{bmatrix} 1 & 0 & 0 & 0 \\ 0 & a & 0 & 0 \\ 0 & 0 & b & 0 \\ 0 & 0 & 0 & c \end{bmatrix} \quad (6)$$

For water surface and volume returns the magnitude of a , b , and c are all approximately 1. In this way the targets are polarization maintaining. However, for rough floor topographies, these terms are generally of magnitude less than 1.

Simulation of the normalized received intensity for targets of varying degrees of vertical linear depolarization, represented as element a in (6), is illustrated in Figure 2. The range of quarter-wave plate orientations from θ_Q of -45 to 45 degrees is provided to the reader for illustration purposes. Light from a polarization-maintaining target ($a=1$) appears sinusoidal, while a completely depolarizing target ($a=0$) produces a constant intensity of 0.5. By translating the quarter-wave plate between orientations θ_Q of 45 and 0 degrees during bathymetric measurements, received signals transition between polarized water surface and volume returns and depolarized floor returns.

Measurements

Bathymetric measurements were made at the University of Colorado, Boulder, using the instrument configuration in Figure 1. The transmitter consisted of a CW-diode pumped passively Q-switched frequency-doubled Nd:YAG microchip laser. The laser outputs 2.45 microjoules of linearly polarized 532 nanometer light at a repetition rate of 14 kilohertz and pulse width of 450 picoseconds. A half-wave plate aligned the laser polarization to the vertical

transmission plane of a 532 nm PBS. Light exiting the PBS transmitted through a quarter-wave plate toward a controlled target consisting of a column of water on top of a depolarizing floor substrate. In this case, ice was used as the floor substrate to replicate expected conditions for depth determination of glacial meltponds.

Backscattered laser light received by the instrument was collected with a photomultiplier tube in photon counting mode. The detector operates with a 1 nanosecond rise time and 350 picosecond timing jitter during output of a 2.5 nanosecond FWHM pulse. Each PMT pulse is passed through a constant fraction discriminator (CFD) which determines the PMT signal apex independently of the signal pulse height. The CFD operates with an intrinsic timing jitter of 3.2 picoseconds, outputting a 2.4 volt TTL-level pulse that is passed to and stored onboard of a time to digital converter (TDC) with 27 picosecond timing resolution.

For demonstration of depth determination, timing data were acquired during reception of backscattered signals from known water depths of 3 and 1 centimeter over ice in an effort to simulate a glacial meltpond shoreline. The transmitted laser pulse was oriented slightly off nadir for collection of water surface and floor returns during each run. In the first data set, the quarter-wave plate was oriented to θ_Q of 45 degrees for reception of polarized surface signals, then translated to 0 degrees to collect backscatter from the depolarizing floor for the second data set. Upon completion of each experiment, the timing data was offloaded to a laptop computer for analysis.

The TDC produces a histogram with a 27 picosecond bin width and one entry per laser firing, allowing for determination of the average time at which the detector pulses are registered. Figure 3 illustrates the surface and floor constant fraction detection histograms for each depth experiment. Visible in Figure 3 is an initial histogram of timing counts extracted from the water

surface returns measured over multiple laser pulses with the quarter-wave plate oriented to θ_Q of 45 degrees. The second histogram is from the floor returns measured over multiple laser pulses with the quarter-wave plate oriented to θ_Q of 0 degrees. Each histogram was normalized to its maximum count value. Each histogram has a spread in time that is due to timing jitter within the system and/or laser pulse width considerations.

Taking into account the refractive index n change of water relative to air (1.33), the water depth h is calculated as

$$h = \frac{c\Delta t}{2n} \quad (7)$$

where the time delay Δt is evaluated by differencing the FWHM timing points of the constant fraction histogram for the surface returns and the constant fraction histogram for the floor returns. The results presented in Figure 3 produce time delays of 247 and 52 picoseconds, corresponding to depth measurements h of 2.7 and 0.6 centimeters, respectively. The 27 picosecond resolution of the TDC imposes a ± 3 millimeter uncertainty on the water depth estimate, placing the observed depths within the uncertainty of the physically measured depths of 3.0 and 1.0 centimeters, which possess a ± 1 millimeter uncertainty.

Discussion

The results presented in Figure 3 demonstrate the reduction of system bandwidth limitations through exploitation of target polarization states. If more traditional bathymetric techniques were employed, given the 450 picosecond laser pulse width and 2.5 nanosecond detector response width, water depths less than tens of centimeters could not be resolved. By isolating detection of surface and floor returns using polarization discrimination, water depth

measurements are limited only by the 27 picosecond resolution of the timing unit. By removing the need for short laser pulses and fast detectors, lasers and detectors with other favorable performance attributes can be used. For instance, lasers of longer pulse width can transmit more energy per pulse and improve the signal-to-noise aspects of the system, lasers of more favorable transmission wavelengths can be utilized, and less expensive lasers and detectors can be employed.

To demonstrate independently the extent of the depth capability of the system, the experiment carried out in the measurement section is revisited. For this experiment, the floor distance remained fixed while 1 and 3 centimeter water depth experiments were executed. Contrasting the setup for each measurement, each floor return in the 3 centimeter water experiment is subject to a transit distance l of 2 centimeters of water compared to floor returns traveling through 2 centimeters of air before entering the 1 centimeter water depth experiment. In this sense, it is expected that the floor return for 3 centimeters of water would be delayed from the floor return for 1 centimeter by a factor Δ of

$$\Delta = \frac{2nl}{c} - \frac{2l}{c} = \frac{2(1.33)(0.02)}{(3 \times 10^8)} - \frac{2(0.02)}{(3 \times 10^8)} = 44 \text{ p sec} \quad (8)$$

due solely to the change in n from water to air over the $2l$ roundtrip distance.

The floor results of each water depth experiment are plotted together in Figure 4. Inset is a zoomed-in view of the FWHM timing points of the trailing edges for the floor return curves corresponding to water depths of 3 and 1 centimeter. Trailing edge values were used primarily due to their repeatability during measurement of known water depths. At an expected Δ of 44 picoseconds, the floor returns for each experiment would be separated by one 27 picosecond timing bin in the digital timing unit.

Differencing the FWHM timing points of the Figure 4 inset demonstrates the returns from the floor of 3 and 1 centimeter water depths are located in neighboring bins, although the timing unit cannot determine their location better than within its 27 picosecond resolution. This measurement comparison demonstrates that the ultimate timing resolution of the technique is dictated by the timing bin width and presently indicates depths could be determined to within millimeters.

Conclusions

Transmission of vertical linearly polarized light through a PBS and translation of a quarter-wave plate modulates received signals between polarized water returns and depolarized floor returns. By exploiting the polarization states of water and floor returns, traditional bathymetry instrument bandwidth limits are reduced. The performance of bathymetric lidars, once confined by laser and/or detector pulse widths, are now limited only by the resolution of timing electronics. The technique presented here has demonstrated 1 centimeter water depth with ± 3 millimeter uncertainty, more than an order of magnitude improvement over previous approaches to bathymetry lidar, with potential for millimeter depth measurement. In addition, reduction of traditional system bandwidth limitations decreases the need for expensive lasers and optical detectors with narrow pulse widths to measure shallow waters. Longer pulses and more optimal laser wavelengths may be used with no consequence on depth determination while potentially improving signal detection. The novel approach can equally be applied to deep water depth measurements, thus providing a complete range of depth determination capabilities.

Acknowledgements

The first author (SM) was supported by the NASA Earth & Space Science Fellowship project #154-5064 and the 2008 CIRES Innovative Research Program project #10652. Coauthors (JT and MH) were supported by NSF grant ATM-0454999. Discussions with SensL Technologies representatives Steven Buckley and David McNally have been instrumental.

References

1. G. Guenther, A. Cunningham, P. LaRoque, and D. Reid, "Meeting the accuracy challenge in airborne lidar bathymetry," in *Proceedings of 20th EARSeL Symposium: Workshop on Lidar Remote Sensing of Land and Sea*, Dresden, Germany, 16-17 June 2000, 28 pp.
2. G. Guenther and R. Thomas, "System design and performance factors for airborne laser hydrography," in *Proceedings Oceans '83*, San Francisco, California, 29 August – 1 September 1983, pp. 425-430.
3. G. Guenther, "Airborne lidar bathymetry" in *Digital Elevation Model Technologies and Applications: The DEM Users Manual*, 2nd Ed., D. Maune, ed. (2007), pp. 253-320.
4. J. Irish and T. White, "Coastal engineering applications of high-resolution lidar bathymetry," *Coastal Engineering*, **35**, 47-71 (1998).
5. A. Nayegandhi, J. Brock, and C. Wright, "Classifying vegetation using NASA's Experimental Advanced Airborne Research Lidar (EAARL) at Assateague Island National Seashore," in *Proceedings ASPRS Annual Conference*, Baltimore, Maryland, 7-11 March 2005, 15 pp.
6. S. Pe'eri and W. Philpot, "Increasing the Existence of Very Shallow-Water LIDAR Measurements Using the Red-Channel Waveforms." *IEEE Transactions on Geoscience and Remote Sensing*, **45**, 1217-1223 (2007).

7. J. Churnside, "Polarization effects on oceanographic lidar," *Opt. Express*, **16**, 1196-1207 (2008).
8. S. Lu and R. Chipman, "Interpretation of Mueller matrices based on polar decomposition," *J. Opt. Soc. Am. A*, **13**(5), 1106-1113 (1996).

List of Figures

Fig. 1 Fundamental setup for polarization shallow water bathymetry.

Fig. 2 Simulation of normalized receive intensity for targets of varying degrees of vertical linear depolarization.

Fig. 3 Normalized digital timing histograms of constant fraction detection for surface and floor returns at 3.0 centimeter (dashed) and 1.0 centimeter (solid) water depths.

Fig. 4 Overlay of normalized surface and floor histograms from Figure 3 along with insert of timing differences between the two determined floor returns.

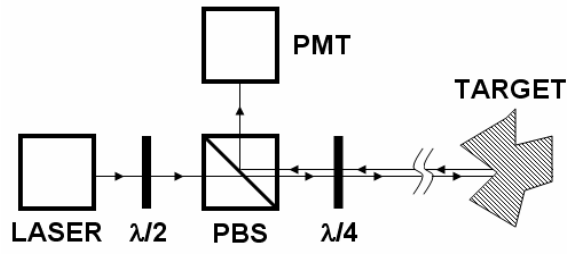


Fig. 1 Fundamental setup for polarization shallow water bathymetry.

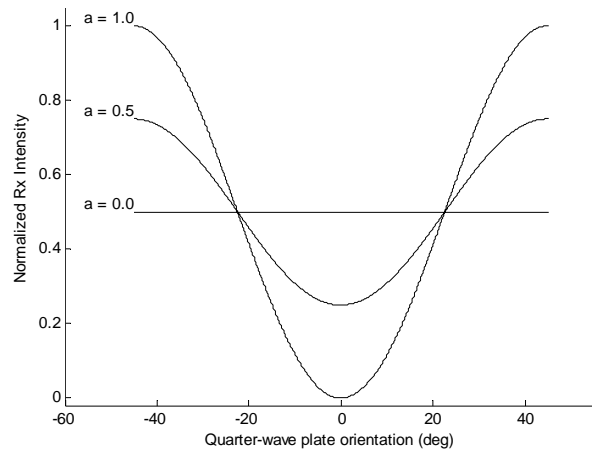


Fig. 2 Simulation of normalized receive intensity for targets of varying degrees of vertical linear depolarization.

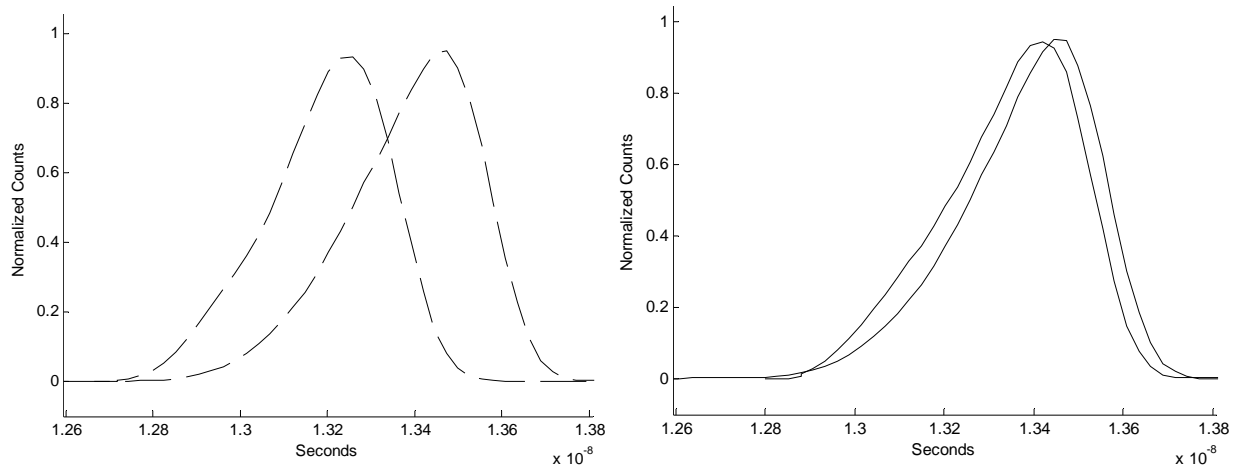


Fig. 3 Normalized digital timing histograms of constant fraction detection for surface and floor returns at 3.0 centimeter (dashed) and 1.0 centimeter (solid) water depths.

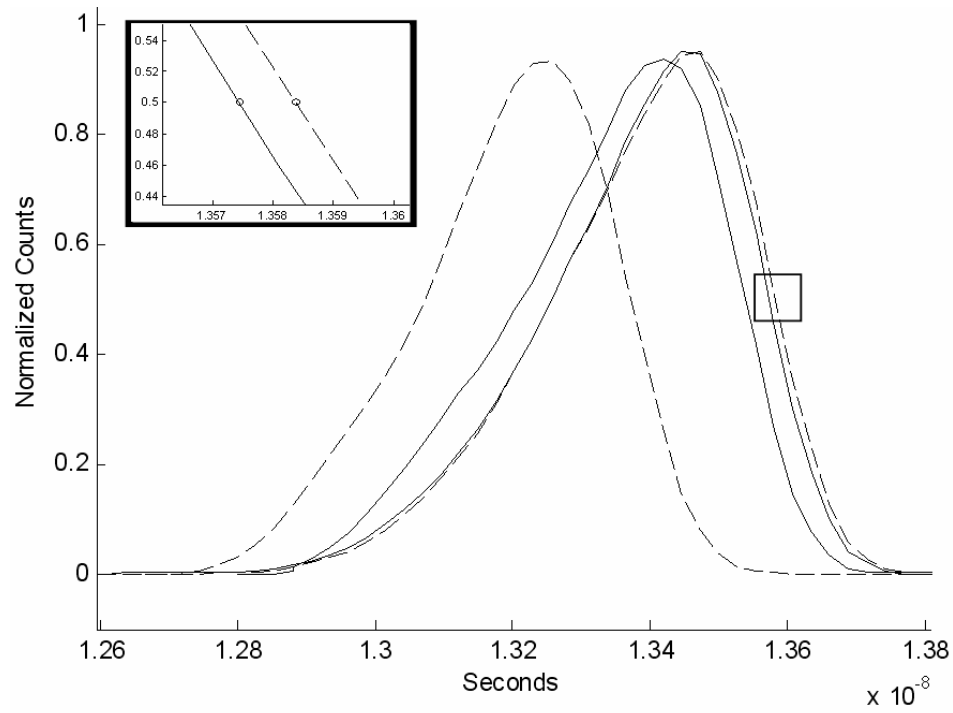


Fig. 4 Overlay of normalized surface and floor histograms from Figure 3 along with insert of timing differences between the two determined floor returns.